Lecture Notes in Computer Science 4057

Commenced Publication in 1973
Founding and Former Series Editors:
Gerhard Goos, Juris Hartmanis, and Jan van Leeuwen

Josien P. W. Pluim
Boštjan Likar
Frans A. Gerritsen (Eds.)

Biomedical Image Registration

Third International Workshop, WBIR 2006
Utrecht, The Netherlands, July 9-11, 2006
Proceedings

Springer

Volume Editors

Josien P. W. Pluim
University Medical Center Utrecht
Image Sciences Institute
Heidelberglaan 100, 3584CX Utrecht, The Netherlands
E-mail: josien@isi.uu.nl

Boštjan Likar
University of Ljubljana
Faculty of Electrical Engineering
Laboratory of Imaging Technologies
Tržaška 25, 1000 Ljubljana, Slovenia
E-mail: bostjan.likar@fe.uni-lj.si

Frans A. Gerritsen
Philips Medical Systems
Healthcare Informatics
P.O. Box 10.000, 5680 DA Best, The Netherlands
and
Technische Universiteit Eindhoven
Department of Biomedical Engineering
The Netherlands
E-mail: frans.gerritsen@philips.com

Library of Congress Control Number: 2006927802

CR Subject Classification (1998): I.4, I.5, H.3, J.3

LNCS Sublibrary: SL 6 – Image Processing, Computer Vision, Pattern Recognition, and Graphics

ISSN 0302-9743
ISBN-10 3-540-35648-7 Springer Berlin Heidelberg New York
ISBN-13 978-3-540-35648-6 Springer Berlin Heidelberg New York

Typesetting: Camera-ready by author, data conversion by Scientific Publishing Services, Chennai, India
Printed on acid-free paper SPIN: 11784012 06/3142 5 4 3 2 1 0

Preface

The Third International Workshop on Biomedical Image Registration (WBIR) was held July 9-11, 2006, at Utrecht University, Utrecht, The Netherlands. Following the success of the first workshop (WBIR 1999), held in Bled, Slovenia, and the second workshop (WBIR 2003), held in Philadelphia, Pennsylvania, this meeting (WBIR 2006) aimed to once again gather leading researchers in the area of biomedical image registration so as to present and discuss recent developments in the field.

In modern medicine and biology, a valuable method of gathering knowledge about healthy and diseased organs, tissues, and cells is the integration of complementary information from volumetric images of these objects. Such information may be obtained by different imaging modalities, different image acquisition setups, different object preparation procedures, or by sequential image acquisition in follow-up studies or in dynamic imaging. A necessary pre-processing step for the integration of image information is image registration by which images, containing complementary information, are brought into the best possible spatial correspondence with respect to each other. Enabling combination and quantification of information about location, form and function, image registration is nowadays finding increasing use in diagnosis, treatment planning, and surgical guidance.

This year's workshop consisted of 20 oral presentations with ample time for discussions, 18 poster presentations and 2 tutorials: one addressing techniques and applications and the other numerical methods for image registration. We were delighted to welcome the participants to Utrecht and hope they found the meeting an interesting, fruitful, enjoyable and stimulating experience. For the readers unable to attend the workshop, we hope that you find these proceedings a valuable record of the scientific programme.

We would like to thank everyone who contributed to the success of this workshop: the authors for their excellent contributions, the members of the Programme Committee for their review work, promotion of the workshop and general support, the tutorial speakers for their outstanding educational contributions, the local organization staff for their precious time and diligent efforts, Philips Medical Systems for kind and generous financial support, and all the attendees for their active participation in the formal and informal discussions.

July 2006

Josien P. W. Pluim
Boštjan Likar
Frans A. Gerritsen

Organization

Chairs

Josien P.W. Pluim	University Medical Center Utrecht, The Netherlands
Boštjan Likar	University of Ljubljana, Slovenia
Frans A. Gerritsen	Philips Medical Systems and Technische Universiteit Eindhoven, The Netherlands

Programme Committee

Daniel Alexander	University College London, UK
Christian Barillot	INRIA, France
Michael Braun	University of Technology, Sydney, Australia
Gary Christensen	University of Iowa, USA
Albert Chung	The Hong Kong University of Science and Technology, Hong Kong
Louis Collins	Montreal Neurological Institute, McGill University, Canada
Benoit Dawant	Vanderbilt University, USA
Bernd Fischer	University of Luebeck, Germany
Mike Fitzpatrick	Vanderbilt University, USA
Jim Gee	University of Pennsylvania, USA
Alexandre Guimond	Siemens Molecular Imaging, UK
Mark Jenkinson	FMRIB Centre, University of Oxford, UK
Tianzi Jiang	National Laboratory of Pattern Recognition, China
Murray Loew	George Washington University, USA
Frederik Maes	K.U. Leuven, Belgium
Twan Maintz	Utrecht University, The Netherlands
Calvin Maurer Jr.	Accuray, Inc., USA
Chuck Meyer	University of Michigan, USA
Sébastien Ourselin	CSIRO ICT Centre, Australia
Xavier Pennec	INRIA, France
Graeme Penney	University College London, UK
Franjo Pernuš	University of Ljubljana, Slovenia
Terry Peters	Robarts Research Institute, London, Canada
Alexis Roche	Service Hospitalier Frederic Joliot, France
Torsten Rohlfing	SRI International, USA
Karl Rohr	University of Heidelberg and DKFZ Heidelberg, Germany
Daniel Rueckert	Imperial College London, UK
Dinggang Shen	University of Pennsylvania, USA

Oskar Škrinjar	Georgia Institute of Technology, USA
Colin Studholme	University of California, San Francisco, USA
Philippe Thévenaz	École Polytechnique Fédérale de Lausanne (EPFL), Switzerland
Max Viergever	University Medical Center Utrecht, The Netherlands
Simon Warfield	Harvard Medical School, USA
Jürgen Weese	Philips Research Laboratories Aachen, Germany
Sandy Wells	Harvard Medical School and Brigham and Women's Hospital, USA

Local Organization

Renee Allebrandi	University Medical Center Utrecht, The Netherlands
Gerard van Hoorn	University Medical Center Utrecht, The Netherlands
Marjan Marinissen	University Medical Center Utrecht, The Netherlands
Marius Staring	University Medical Center Utrecht, The Netherlands
Jacqueline Wermers	University Medical Center Utrecht, The Netherlands
Darko Škerl	University of Ljubljana, Slovenia

Sponsoring Institution

Philips Medical Systems, The Netherlands PHILIPS

Table of Contents

Medical Image Registration Based on BSP and Quad-Tree Partitioning

A. Bardera, M. Feixas, I. Boada, J. Rigau, and M. Sbert

Institut d'Informàtica i Aplicacions, Universitat de Girona, Spain
{anton.bardera, miquel.feixas, imma.boada,
jaume.rigau, mateu.sbert}@udg.es

Abstract. This paper presents a study of image simplification techniques as a first stage to define a multiresolution registration framework. We propose here a new approach for image registration based on the partitioning of the source images in binary-space (BSP) and quad-tree structures. These partitioned images have been obtained with a maximum mutual information gain algorithm. Multimodal registration experiments with downsampled, BSP and quadtree partitioned images show an outstanding accuracy and robustness by using BSP images, since the grid effects are drastically reduced. The obtained results indicate that BSP partitioning can provide a suitable framework for multiresolution registration.

1 Introduction

Multimodal image registration plays an increasingly important role in medical imaging. Its objective is to find a transformation that maps two or more images, acquired using different imaging modalities, by optimizing a certain similarity measure. Among the different similarity measures that have been proposed, mutual information (MI)[2, 9] and normalized mutual information (NMI)[6] are the most commonly used since they produce satisfactory results in terms of accuracy, robustness and reliability. However, MI-based methods are very sensitive to implementation decisions, such as interpolation and optimization methods, and multiresolution strategies [4]. The latter allow us to reduce the computational cost by means of a coarse-to-fine hierarchical representation of the images. Crucial to building these hierarchies is the selection of the image simplification strategy.

The main objective of this paper is to analyze the behavior of the registration process when the source images are simplified in BSP and quad-tree structures, obtained with a maximum MI gain algorithm [5]. We will see that multimodal registration experiments based on BSP partitioned images show a remarkable accuracy and robustness, reducing substantially the grid effects compared with both regular downsampled and quad-tree images. Since experimental results demonstrate the good performance using these simplification strategies, we suggest they are an ideal strategy for defining a multiresolution framework. Such a framework can be used not only for registration purposes but also for image processing or transmission in telemedicine environments.

J.P.W. Pluim, B. Likar, and F.A. Gerritsen (Eds.): WBIR 2006, LNCS 4057, pp. 1–8, 2006.

This paper is organized as follows. In Section 2, we briefly describe image registration and partitioning techniques using MI maximization. In Section 3, a new image registration framework based on partitioned images is presented. In Section 4, multimodal registration experiments show the suitability of the presented approach. Finally, our conclusions are given in Section 5.

2 Previous Work

In this section we review the MI definition [1] and its application to image registration [2, 9, 4, 7] and partitioning [5].

Mutual Information. Given two discrete random variables, X and Y, with values in the sets $\mathcal{X} = \{x_1, \ldots, x_n\}$ and $\mathcal{Y} = \{y_1, \ldots, y_m\}$, respectively, the MI between X and Y is defined as

$$I(X,Y) = \sum_{i=1}^{n} \sum_{j=1}^{m} p_{ij} \log \frac{p_{ij}}{p_i q_j} \tag{1}$$

where $n = |\mathcal{X}|$, $m = |\mathcal{Y}|$, $p_i = Pr[X = x_i]$ and $q_j = Pr[Y = y_j]$ are the marginal probabilities and $p_{ij} = Pr[X = x_i, Y = y_j]$ is the joint probability. $I(X,Y)$ is a measure of the shared information between X and Y. It can also be expressed as $I(X,Y) = H(X) - H(X|Y) = H(Y) - H(Y|X)$, where $H(X)$ and $H(Y)$ are the marginal entropies, and $H(X|Y)$ and $H(Y|X)$ the conditional entropies [1].

A fundamental property of MI is the *data processing inequality* which can be expressed in the following way: if $X \rightarrow Y \rightarrow Z$ is a Markov chain, then

$$I(X,Y) \geq I(X,Z). \tag{2}$$

This result demonstrates that no processing of Y, deterministic or random, can increase the information that Y contains about X [1].

MI-based Image Registration. The most successful automatic image registration methods are based on MI, which is a measure of the dependence between two images. The registration of two images is represented by an information channel $X \rightarrow Y$, where the random variables X and Y represent the images. Their marginal probability distributions, $\{p_i\}$ and $\{q_j\}$, and the joint probability distribution, $\{p_{ij}\}$, are obtained by simple normalization of the marginal and joint intensity histograms of the overlapping areas of both images [2]. The registration method based on the maximization of MI, almost simultaneously introduced by Maes et al. [2] and Viola et al. [9], is based on the conjecture that the correct registration corresponds to the maximum MI between the overlapping areas of the two images. Later, Studholme et al. [6] proposed a normalization of MI defined by

$$NMI(X,Y) = \frac{H(X) + H(Y)}{H(X,Y)} = 1 + \frac{I(X,Y)}{H(X,Y)}, \tag{3}$$

which is more robust than MI, due to its greater independence of the overlap area.

The behavior of the MI-based method depends on the implementation decisions. Thus, for instance, it is especially sensitive to the interpolator and optimizator chosen or the binning and multiresolution strategies [4]. Generally the grid points of the transformed image do not coincide with the grid points of the reference image. Thus, the selection of an interpolator is required. Although there are different interpolators, all of them introduce artifacts due to the error patterns caused by the grid regularity [7]. On the other hand, the simple computation of an MI-based similarity measure by sampling the images on a regular grid leads to undesired artifacts, called *grid effects* [8].

MI-Based Partitioning Algorithm. An MI-based algorithm was presented by Rigau et al. [5] to partition an image. Given an image with N pixels and an intensity histogram with n_i pixels in bin i, a discrete information channel $X \rightarrow Y$ is defined, where X represents the bins of the histogram, with marginal probability distribution $\{p_i\} = \{\frac{n_i}{N}\}$, and Y the image partitioned into pixels, with uniform distribution $\{q_j\} = \{\frac{1}{N}\}$. The conditional probability distribution $\{p_{j|i}\}$ of this channel is defined as the transition probability from bin i of the histogram to pixel j of the image, and vice versa for $\{p_{i|j}\}$. This channel fulfills that $I(X,Y) = H(X)$ since, knowing the output (pixel), there is no uncertainty about the input bin of the histogram. From the data processing inequality (2), any clustering or quantization over X or Y, respectively represented by $\widehat{X}$ and $\widehat{Y}$, will reduce the MI of the channel. Thus, $I(X,Y) \geq I(X,\widehat{Y})$ and $I(X,Y) \geq I(\widehat{X},Y)$.

From the above reasonings, a pixel clustering algorithm which minimizes the loss of MI could be proposed. However, its high cost suggests adopting the contrary strategy, where the full image is taken as the unique initial partition and is progressively subdivided according to the maximum MI gain for each partitioning step. This algorithm is a greedy top-down procedure which partitions an image in quasi-homogeneous regions. This method can be visualized from equation $H(X) = I(X,\widehat{Y}) + H(X|\widehat{Y})$, where the acquisition of information increases $I(X,\widehat{Y})$ and decreases $H(X|\widehat{Y})$, producing a reduction of uncertainty due to the equalization of the regions. Different stopping criteria can be used. For more details, see [5].

3 Registration from Partitioned Images

Registration aims to find a transformation which maps two or more images by optimizing certain similarity measure. Multiresolution and multisampling strategies can be used to reduce its computational cost by means of a coarse-to-fine hierarchical strategy which starts with the reference and floating images on a coarser resolution. The estimates of the correspondence or parameters of the mapping functions while going up to finer resolutions are progressively improved. At every level they considerably decrease the search space and thus save computational time. In particular, downsampling techniques cause a great acceleration of the registration process [4].

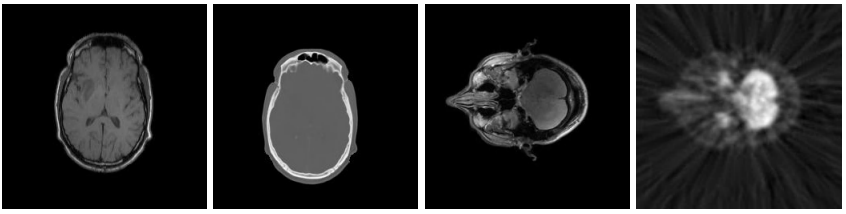

(*a*) MR (*b*) CT (*c*) MR (*d*) PET

Fig. 1. Test images from the Vanderbilt database [3]

Obviously, a good strategy to speed-up the registration process could be to use simplified images instead of the original ones. Our proposal is to register the images obtained with the MI-based partitioning algorithm presented in Sec. 2. These images contain a high information level for a reduced number of regions. This proposal is a first approximation for considering the benefits of a multiresolution approach which would consist in the interplay of the different resolutions of both images to accelerate registration. At each registration level, the best suited resolution for each image would be selected. Crucial to developing this multiresolution framework is the selection of the simplification strategy that has to be applied to simplify images. In this paper, we investigate two subdivision techniques, BSP and quadtree, to determine which provides better results.

To carry out this study, we propose a two step registration process. In the first step, the original images are progressively partitioned with vertical or horizontal

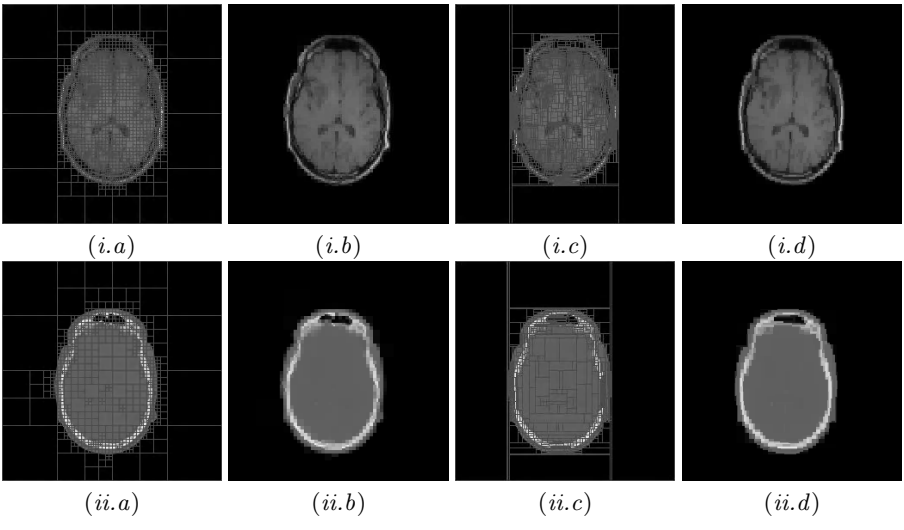

(*i.a*) (*i.b*) (*i.c*) (*i.d*)

(*ii.a*) (*ii.b*) (*ii.c*) (*ii.d*)

Fig. 2. (*i*) MR and (*ii*) CT images obtained from Fig. 1(*a*-*b*). (*a*) Quad-tree partitions with $MIR = 0.7$, (*b*) quad-tree simplified images, (*c*) BSP partitions with $MIR = 0.7$, and (*d*) BSP simplified images.

Table 1. Percentage of regions obtained with respect to the initial number of pixels corresponding to MR and CT original images of Fig. 1(*a-b*) and for a given MIR

MIR	MR		CT	
	BSP	quad-tree	BSP	quad-tree
0.5	0.25	0.40	0.06	0.13
0.6	0.81	1.18	0.21	0.39
0.7	2.21	3.16	0.77	1.28
0.8	5.28	6.56	2.73	3.87
0.9	11.88	16.05	7.98	11.48

lines (BSP) or with a quad-tree structure. In both cases, an MI ratio given by $MIR(X,\widehat{Y}) = \frac{I(X,\widehat{Y})}{H(X)}$ is used as a stopping criterion. This ratio is a measure of the simplification quality.

In Fig. 2 we illustrate the behaviour of this partitioning step applying it to the 2D MR-CT pair of images (Fig. 1(*a-b*)). In Fig. 2(a,c) we show for each original image the partitioning lines of the quad-tree and BSP structures and in Fig. 2(b,d) the corresponding *simplified* images obtained by averaging for each region the intensity of its pixels. We also collect in Table 1 the percentage of regions obtained with the simplification with respect to the initial number of pixels corresponding to the original MR and CT images. Note that a big gain of MI is obtained with a relative low number of partitions. Thus, for instance, in the CT case, a 70% of MI ($MIR = 0.7$) is obtained with approximately 1% of the maximum number of partitions (number of pixels of the source image). Observe that less partitions are needed in the CT image to extract the same MIR than in the MR image. This is due to the fact that the higher the image homogeneity, the higher the degree of simplification. In this example, the CT image is more homogeneous than the MR image.

In the second step of the process, the previously partitioned images are registered using the NMI metric and the Powell's algorithm as optimizer. To illustrate the feasibility of this proposal, we have registered simplified images of the MR-CT of Fig. 1(*a-b*), considering first an MIR of 0.6 and then an MIR of 0.7. The registration results are shown in Fig. 3, where, respectively, (a) and (b) correspond to $MIR = 0.6$ and $MIR = 0.7$, and (i) and (ii) to the quad-tree and BSP partitioned images. In this figure, to illustrate better the obtained results, we apply the transformation obtained from the registration of the simplified images to the original ones. In addition, for each one of these images we compute the translational error (t_x,t_y). We consider the registration result of the original images without any partitioning process as being correct, so this error measures the deviation in x and y translation between the transformation corresponding to the correct registration and the evaluated one. In all the cases, the rotational error has been omitted due to its insignificant value. Observe that BSP images with $MIR = 0.6$ (Fig. 3($ii.a$)) achieve a lower error than quad-tree images with $MIR = 0.7$ (Fig. 3($i.b$)). This demonstrates that better results are obtained with the registration of the BSP partitioned images.

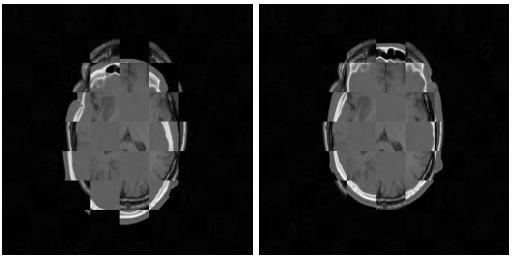

($i.a$) (5.64, 16.33) ($i.b$) (2.38, 0.36)

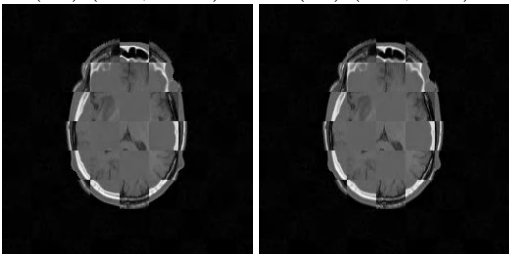

($ii.a$) (0.36, 0.71) ($ii.b$) (0.36, 0.17)

Fig. 3. Registration for the MR-CT pair of Fig. 1(a-b). (i) Quad-tree and (ii) BSP subdivision methods for (a) $MIR = 0.6$ and (b) $MIR = 0.7$. The translational error (t_x,t_y) is shown for each registration.

4 Results and Discussion

In order to evaluate more accurately the performance of the registration of MI-based partitioned images, experiments on MR-CT (Fig. 1(a-b)) and MR-PET (Fig. 1c-d) images are presented. In these experiments, the corresponding pair of images have the same degree of simplification, i.e., an MR quad-tree (or BSP) image with $MIR = 0.7$ is registered with a CT quad-tree (or BSP) with the same MIR. These results are compared with regular downsampled images.

In Fig. 4 the results of our experiments are presented. The behavior of the NMI measure is analyzed moving the floating image one pixel at each step through the X axis from -100 to 100 pixel units around the origin. No interpolation artifacts appear since there is no pixel interpolation. In all the plots, the bottom curve corresponds to the NMI registration of the source images. The MR-CT and MR-PET results are shown in the first (i) and second (ii) rows, respectively. In Fig. 4 (a), we illustrate the NMI measure obtained with different downsamplings of the original images. From bottom to top, the NMI curves correspond to downsampling of 2×2, 4×4, 8×8 and 16×16 pixels, respectively. Note that, high artifacts appear at every n pixels coinciding with the downsampling factor. In Fig. 4(b-c), we illustrate the NMI values for the quad-tree and BSP partitioned images, respectively. Each curve corresponds to a different degree of simplification. From bottom to top, MIR ranges from 0.9 to 0.5. Observe in Fig. 4(b) that the quad-tree partition also produces correlation artifacts due to the regularity

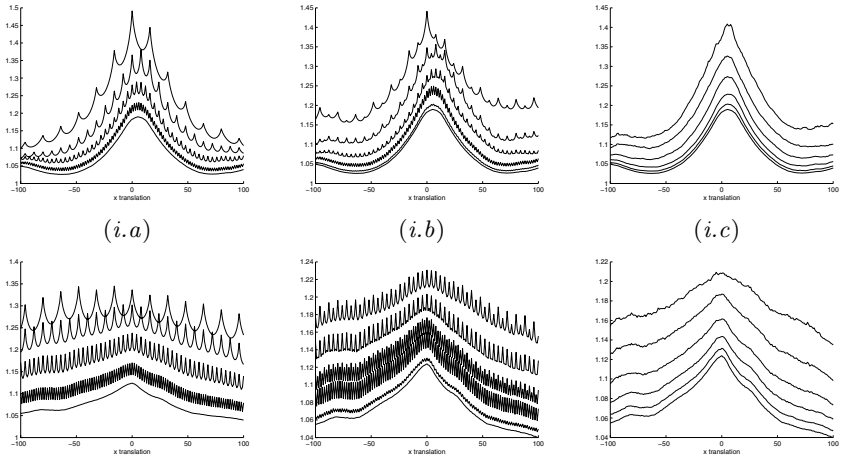

Fig. 4. (i) MR-CT (Fig. 1(a-b)) and (ii) MR-PET (Fig. 1(c-d)) registration results corresponding to (a) downsampled, (b) quad-tree, and (c) BSP images. The horizontal axis represents the slice translation on the X-axis (in pixels) and the vertical axis the value of NMI. For each plot, the NMI measure for different degrees of downsampling (a) and simplification (b-c) of the images are shown.

of its partitions. However, these artifacts are slightly reduced with respect to the downsampling case, since, although the registered images have the same degree of simplification, the number and the position of the generated quad-tree partitions are not the same.

Finally, in Fig. 4(c) we analyze the BSP partition. In this case, the grid artifacts are nearly completely eliminated since neither the position nor the number of partitions of the images coincide. Registration is more robust since the probability of finding a local maximum is lower as it is shown by the smoothness of BSP plots. Taking into account that the perfect registration is given by the maximum bottom curve, observe the high accuracy, i.e., the coincidence of the curve maxima, of the registration reached with the BSP images. For instance, an accurate registration is achieved with $MIR = 0.7$, which represents an approximate reduction of 99% of the original number of pixels.

Experiments with the MR-PET images shown in Fig. 4(ii) behave similarly to the MR-CT case in Fig. 4(i). In both cases, the BSP simplification scheme behaves considerably better than both quad-tree simplification and downsampled images in terms of the reduction of grid artifacts. From these experiments we can conclude that the BSP approach is more robust and accurate.

5 Conclusions and Future Work

In this paper, we have presented a new technique for image registration based on the partitioning of the source images. Thepartitioning algorithm relies on the

maximization of the mutual information gain for each refinement decision. The presented method is a first step towards a full multiresolution registration approach. Two alternatives (binary space partition and quad-tree simplifications) have been analyzed and compared with a usual regular downsampling technique. The quality of the subdivision has been investigated in terms of the efficiency in registration. Results have shown the superior quality of the BSP subdivision, which allows a smoother registering. The BSP approach performs also better than regular downsampling. The next step in our research will consist in developing a multiresolution framework using the BSP subdivision.

Acknowledgments

The images used in our experiments were provided as part of the project, "Evaluation of Retrospective Image Registration", National Institutes of Health, Project Number 1 R01 NS33926-01, Principal Investigator Prof. J. Michael Fitzpatrick, Vanderbilt University, Nashville, TN. This project has been funded in part with grant numbers TIN2004-08065-C02-02, TIN2004-07451-C03-01 and 2001-SGR-00296.

References

1. Thomas M. Cover and Joy A. Thomas. *Elements of Information Theory.* Wiley Series in Telecommunications, 1991.
2. F. Maes, A. Collignon, D. Vandermeulen, G. Marchal, and P. Suetens. Multimodality image registration by maximization of mutual information. *IEEE Transactions on Medical Imaging*, 16(2):187–198, 1997.
3. National Institutes of Health. *Retrospective Image Registration Evaluation.* Vanderbilt University, Nashville (TN), USA, 2003. Project Number 8R01EB002124-03, Principal Investigator J. Michael Fitzpatrick.
4. Josien P.W. Pluim, J.B.A. Maintz, and M.A. Viergever. Mutual-information-based registration of medical images: a survey. *IEEE Transactions on Medical Imaging*, 22:986–1004, 2003.
5. J. Rigau, M. Feixas, M. Sbert, A. Bardera, and I. Boada. Medical image segmentation based on mutual information maximization. In *International Conference on Medical Image Computing and Computed Assisted Intervention (MICCAI 2004), Proceedings*, Rennes-Saint Malo, France, September 2004.
6. Colin Studholme. *Measures of 3D Medical Image Alignment.* PhD thesis, University of London, London, UK, August 1997.
7. J. Tsao. Interpolation artifacts in multimodal image registration based on maximization of mutual information. *IEEE Transactions on Medical Imaging*, 22:854–864, 2003.
8. M. Unser and P. Thévenaz. Stochastic sampling for computing the mutual information of two images. In *Proceedings of the 5th International Workshop on Sampling Theory and Applications (SampTA'03)*, pages 102–109, Strobl, Austria, May 2003.
9. Paul A. Viola. *Alignment by Maximization of Mutual Information.* PhD thesis, Massachusetts Institute of Technology, Massachusetts (MA), USA, 1995.

A Bayesian Cost Function Applied to Model-Based Registration of Sub-cortical Brain Structures

Brian Patenaude, Stephen Smith, and Mark Jenkinson

FMRIB Centre, University of Oxford

Abstract. Morphometric analysis and anatomical correspondence across MR images is important in understanding neurological diseases as well as brain function. By registering shape models to unseen data, we will be able to segment the brain into its sub-cortical regions. A Bayesian cost function was derived for this purpose and serves to minimize the residuals to a planar intensity model. The aim of this paper is to explore the properties and justify the use of the cost function. In addition to a pure residual term (similar to correlation ratio) there are three additional terms, one of which is a growth term. We show the benefit of incorporating an additional growth term into a purely residual cost function. The growth term minimizes the size of the structure in areas of high residual variance. We further show the cost function's dependence on the local intensity contrast estimate for a given structure.

1 Introduction

Morphometric changes in sub-cortical brain regions are associated with psychiatric disorders, neurodegenerative diseases, and aging. Furthermore, anatomical correspondence across MR images is needed to perform group analysis of functional data. Manual delineation of subcortical structures is a very time consuming task and requires considerable training. One approach to solving this problem is by registering a probabilistic brain atlas to new data [1]; a more recent approach also incorporates anisotropic Markov Random Fields and intensity priors [2]. We are proposing to solve the registration/segmentation problem by registering statistical shape models to MRI data.

A Bayesian similarity function which aims to minimize the residuals to a planar intensity model was derived to drive the registration. The aim of this paper is to investigate the cost function's properties and justify its use. Like correlation ratio, this cost function minimizes residuals, however it has three additional terms. We show that the added benefit of the full Bayesian cost function over a pure residual function is due to the addition of a growth term. The balance between the growth and residual term is governed by the local intensity contrast for a given structure. The cost function's relationship to the local intensity contrast is examined as well.

J.P.W. Pluim, B. Likar, and F.A. Gerritsen (Eds.): WBIR 2006, LNCS 4057, pp. 9–17, 2006.

2 Methods

2.1 Model Building

The training set consisted of 93 manually labelled T1-weighted MRI brain scans (courtesy of the CMA in Boston). The labelling is of a high quality and their reliability and reproducibility have been documented [3, 4]. As a first step, the training data are first affine-registered to MNI152 space. The training points are then automatically assigned to the manually labelled data using deformable surfaces. Within-surface motion constraints are imposed on the deformation process to preserve point correspondence. We assume a multivariate Gaussian model, and estimate its parameters using PCA [5, 6].

Figure 1a shows the average mesh for the left putamen, pallidum, and thalamus (three sub-cortical brain structures), which are used to initialize the registration. The transformations are applied directly to the model surface meshes, which are then converted into image space for evaluation. The conversion to image space is discussed in more detail in the following section. The deformations are limited to linear combinations of the modes of variation, and are proportional to the cost-gradient in the direction of the modes of variation. Figure 1b shows the first three modes of variation for the left putamen.

2.2 Cost Function

Relating the surfaces to an MRI image is done using a Bayesian similarity function that was derived specifically for this purpose. It is expressed in terms of the posterior probability of a transformation T (the deformation of the surface models) given the observed MR intensity data, Y, and the statistical shape model, S. In its negative log-likelihood form it acts as a cost function and has the form:

$$F_B = -\log\left(p(T|Y,S)\right) \propto -\log\left(p(T)\right) + \frac{1}{2}\log\left|\det\left(G_{in}^T G_{in}\right)\right| \\ -\log\left(\Gamma\left(\frac{N_{eff}}{2}-1\right)\right) + \frac{N_{eff}}{2}\log\left(\pi C^{-2} Y^T R Y\right) \quad (1)$$

where $p(T)$ is the prior probability of a transformation (based on the statistical shape model), G_{in} is the image generator matrix (whose columns are reshaped model intensity images – see below), N_{eff} is the effective number of voxels in the shapes of interest (degrees of freedom), C is an estimate of the local intensity contrast, $Y^T RY$ is the residual variance in the area of interest, where R is a residual forming matrix. This similarity function (described more fully in [7, 8]) is based on the principle of an image generation function that relates the surfaces to images with voxel intensities. By fitting a model to the image intensities within the mesh region, an intensity image is generated according to the parameter estimates of the model. The particular form of image generation function chosen is one that allows the voxels within an image to have a constant intensity plus three spatially-linear gradient terms. That is, a planar fit in intensity is done within the voxels bounded by each surface (with appropriate allowance for partial